Deformation mechanism of Area C landslide in Suijiang, Xiangjiaba Reservoir, Yunnan Province, China

Fuchu Dai[a,b], Wenping Dong[a,*], Zhiquan Huang[a], Jiahua Lei[a], Hongying Zhang[b]

[a]*School of Resources and Environment, North China University of Water Resources and Electric Power, Zhengzhou 450045, China, email: 812971359@qq.com (W. Dong)*
[b]*Key Laboratory of Urban Security and Disaster Engineering, Beijing University of Technology, Beijing 100124, China*

ABSTRACT

The Xiangjiaba project is located in the Shuifu County, Yunnan Province. It is situated approximately 157 km away from the Xiluodu project, 33 km away from the Yibin City and 1.5 km away from the Shuifu County. The Area C landslide of Suijiang County, with a volume of 47 million m³, is located on the southern bank of the Xiangjiaba project. The landslide body has been experiencing persistent deformation with a recorded maximum horizontal displacement of 1,480 mm up to December 2015, posing a critical threat to the lives and properties of local residents. Based on the data collected from detailed geological surveys and three-year monitoring, this paper presents the findings of an in-depth study about deformation characteristics and influence factors of Area C landslide. The findings indicate that: the high southern terrain, steep back rock, wavy-bedded sandstone and mudstone interbeds and hydrophilic soil provide necessary conditions for the landslide. The Area C is located in ancient landslide sites, a secondary shear exists in its front. During the rainy season, the displacement rate of Area C increased sharply, and the deformation is more closely associated with the sudden drop of reservoir water than with the sudden rise. The safety factor decreases under reservoir inundation and rainfall. Continuous creep contributes to the movements of Area C landslide, though the movements are slow. The possibility of high-speed slip is very small. Relevant measures should be taken to protect the safety of lives and properties of the immigrants.

Keywords: Landslide; Deformation mechanism; Rainfall; Reservoir water

1. Introduction

The instabilities of bank slope induced by heavy rainfall and reservoir inundation have attracted worldwide attention in the sector of hydraulic and hydropower engineering. In October 1963, a large-scale landslide of Vajont Reservoir in Italy slipped with a volume of 270 million m³. The landslide was triggered by the changes of reservoir water level and caused 2,500 to 2,600 deaths [1,2]. From 1965 to 1969, the Cepatsch Dam in Austria slipped about 10 m during reservoir inundation [3]. The landslide of Llobregat River Basin in Spain, the deformation patterns altered in accordance with different rainfall intensity [4]. In 2000, the Liguria Region of Imperia Province in Italy slipped with a displacement of more than 1,000 mm in 45 d due to heavy rainfall [5]. In China, several catastrophic landslides occurred near Three Gorges Reservoir [6]. Taking the Jipazi landslide in Yunyang, Chongqing as an example, heavy rains reactivated an ancient landslide site affecting a total volume of 150 million m³ in 1982 [7]. Caused by fragile geological structure and rainfall intensity, the Qianjiangping landslide occurred in Zigui, Hubei, leading to a death toll of 14 with 10 missing in 2003 [8,9]. The Baishui River landslide, with a volume of 12.6 million m³, was triggered by heavy rainfall and reservoir water,

---

* Corresponding author.

then blocked the road in 2007 [10,11]. In June 2007, rainfall and the drop of reservoir water caused the Baijiabao landslide slipped with a volume of 9.9 million m³ [12,13]. The Shuping landslide began to deform as soon as the Three Gorges Reservoir impounded in 2003, and the change of reservoir water and heavy rainfall accelerated the deformation [14–16]. Affected by heavy rainfall and decrease of reservoir water, the Woshaxi landslide caused persistent deformation; the Gongjiafang landslide in Wushan and the Bazimen landslide in Zigui, which were affected by reservoir water and heavy rainfall, caused great deformation in 2009 [12,17,18]. Fortunately, no losses were incurred to person or property thanks to timely monitoring and early warning. Affected by rainfall intensity and the drop of reservoir water, the Outang landslide slipped with a volume of 90 million m³, threatening the lives and properties of about 3,900 people [19].

The Xiangjiaba project is the last power station for the planning of cascade hydropower projects on the Jinsha River [20–25]. It serves as the major project of China's implementation of the "West-East Power Transmission Project", which supplies electricity to the central and eastern parts of China, along with the Sichuan, Chongqing, and Yunnan Provinces. The project is located in Shuifu County, Yunnan Province, about 157 km from the Xiluodu dam, 33 km from the Yibin City and 1.5 km from Shuifu County (Fig. 1). The reservoir has a normal pool level (NPL) of 380 m and a total capacity of 5.158 billion m³. The backwater of the reservoir is 156.6 km long. A total of 47 landslides, totaling 227 million m³ in volume were identified.

The northern terrain of the new Suijiang County is higher than the south, which is between the Dawen Creek and Xiaowen Creek extending from the east to the west along the right bank of the Jinsha River. It is divided by Xiaoxi gully and Sifangbei gully into Area A, B, and C from the upstream of the Jinsha River. In early 2011, Area C was leveling up for construction, and the housing construction reached its peak in the same year. In August 2012, the resettlement housing was delivered to immigrants. However, 1 month later, in September, cracks occurred in the floors and walls of some buildings. After impounding the reservoir to the NPL of 380 m in September 2013, cracks appeared in the retaining plates of anti-slide piles in March 2014, and then in other

parts of Area C in July 2014, which seriously undermined the safety of lives and properties. Therefore, based on the data of detailed geological survey and three-year monitoring of the Area C, this paper offers an in-depth analysis about the deformation mechanism, and the impact of heavy rainfall and reservoir water changes on landslide occurrences.

2. Overview of the landslide site

The Area C is located in the east of new Suijiang county, with Sifangbei Gully in the west, the Xiaowen Creek in the east and Jinsha River in the north. It is situated before a high mountain in the south, and there is a Jinjiang Road at the foot of the mountain. The southern terrain is higher than the north. It is divided into five parts: Area LMG, Area CP1, Area CP2, Area GBP1, Area GBP2, and Area GBP3. According to the monitoring data, the findings could be summarized as follows: (1) relatively stable areas: Area CP2, Area GBP2, Area GBP3; (2) Active areas: Area LMG, Area CP1, and Area GBP1. Table 1 illustrates the relevant indicators of measuring points with maximum horizontal displacement in different areas.

The active areas cover an area of about 56 ha, and an estimated volume of 47 million m³. The landslide has a maximum longitudinal length of 2,300 m from north to south and a maximum width of 1,500 m from east to west. There are two deep gullies developed in Area C, namely the No. 7 Gully and the LMG Gully. The No. 7 Gully runs through the whole area with a depth of 3–10 m, and the gully reaches a depth of 20 m in the end. Cracks near the gully are easy to identify, with a trend of NNW-NNE (Ex. LF17). Some cracks reveal dilatant feature. The LMG Gully has a depth of 35 m. Some cracks near the gully have a trend of NE, nearly in line with that of gully itself (Ex. LF7-1, LF7-2). The cracks cover from the north of gully to the south of Jinjiang Road. The cracks, close to the anti-slide piles which are next to Jinjiang Road, demonstrate clearly the left rotational shearing. To the left of LMG Gully there are many NE trend cracks (Ex. LF21), whereas to the right of LMG Gully, next to anti-slide piles D of Jinjiang Road, some cracks occurred during the excavation and demonstrated no evident development thereafter. There are many EW cracks in Area GBP1 stretch to the elevation

Fig. 1. Location of the Xiangjiaba reservoir.

Table 1
Indices of maximum measuring points in active zones

Area	Maximum deformation rate (mm d^{-1})	Monitoring point	Horizontal displacement (mm)	Vertical displacement (mm)
LMG	4. 13	TPL29	948	155
CP1	2. 14	TPC23	848	218
GBP1	3. 84	TPC18	1,480	545

about 610 m, some of those cracks are NW (Ex. LF28-1, LF28-2) (Fig. 2).

The outcropped strata in Area C include the quaternary system and upper Shaximiao Formations of Mid Jurassic (J_{2s}). The quaternary system include man-made deposit (Q_4^S), alluvium (Q_4^{pal}), and colluvium (Q_4^{codl}): (1) Man-made deposit (Q_4^S): mainly new filled earth such as silt clay blocks, rubbles, etc. with a thickness of 0–23 m; (2) The alluvium (Q_4^{pal}): mainly composed of cobble and gravel, blocks and detritus with sand inclusion, with a thickness of 3–10 m; (3) The colluvium (Q_4^{codl}): mainly composed of silt clay blocks and rubbles, loose shallow soil and high density deep soil, the thickness is 30–50 m, and a maximum thickness of 100 m; (4) The J_{2s} of Jurassic system: mainly composed of purple red and gray purple mud rocks, siltstones and quartz sandstones interbed.

The Area C is a bedding landslide. The altitude of rock in the north of TPC23 is 10°–30°/NW∠3°–25°, and the rock in the south is 10°–50°/NW∠20°–45°. The stratigraphic joint develops well, especially for net fractures in intense-weathered mudstones whose joints are short and small, and dip angle is very steep and filled with argillaceous sediment. Our findings extracted from survey and drilling demonstrate that muddy intercalations and crushing intercalations in the deep bed rock develop well. The muddy intercalations are mainly composed of orange-yellow mudstone debris intercalations, with same shape of clay, and turn into flow plastic or soft flow plastic when they encounter water. And the crushing intercalations are composed of sandstones, mudstone fragments, and orange-yellow mud intercalations, which are strong weathering. The total clay minerals content in muddy intercalations could be 40% with poor permeability, which are easy to be softened with water. The muddy intercalations JC1–JC4 cover an excessive length.

There are 28 measuring points in active areas of Area C, 12 on the surface of Area LMG, 7 on the surface of Area CP1, and 9 on the surface of Area GBP1. In addition, 44 inclinometers are set up in active area, of which 12 are located in the Area LMG, 12 in the Area CP1, and 20 in the Area GBP1. Based on the data of measuring points and inclinometer, we can determine the A-A′ section as the main sliding surface (Fig. 3), whose data and curves of inclinometers are shown in Table 2 and Fig. 4.

Five sets samples (S1–S5) were collected from the main sliding zone for test. Several scratches and mirror planes are visible in the undisturbed samples. It comprises of 64%–76% of illite/smectite and 14%–19% of illite. The grain size distribution curves of samples are illustrated in Fig. 5. Saturated ring shear test of disturbed samples were conducted. The results indicate that the cohesion of residual strength is 10.3 kPa, and the frictional angle is 12.8°. The safety factor

before reservoir inundation and heavy rainfall is 1.2, while the safety factor would drop to 0.99 thereafter.

3. Deformation characteristics of the landslide

In August 2012, several cracks LF4-LF6 first appeared in LMG Gully. In October 2013, LF23 were found in the center of Jinjiang Road, with a length of 20 m and a width of 3–5 cm The Jinjiang Road cracked later again for several times after being overhauled. In July 2014, LF21 and LF22 emerged. The former one consisted of 8–12 parallel cracks, and the trend was close to NS. The latter one consisted of 4–6 parallel cracks with an angle of N 30°E. Both cracks showed no obvious changes subsequently.

In March 2014, cracks emerged in the retaining plates and the top beam of anti-slide piles C in Area GBP. After repairing in October, cracks occurred once again. In July 2014, the retaining plates of anti-slide piles B cracked. In December 2015, the cracks next to anti-slide piles passed through the top beam, the retaining plates and the road. In July 2014, the cracks of LF28-1 and LF28-2 were about 3–5 cm, and in December 2015, they stretched to about 25 cm.

In July 2014, cracks LF17 were found in Area CP1, with a width of 5 cm. In March 2015, the cracks expanded to about 15 cm, and a subsidence was revealed at its east. In July 2014, LF18-1 was found with a maximum width of about 5 cm, and later the cracks were multiplied. In December 2015, the width of cracks at the center of Area CP1 (LF20-1, LF20-2, LF10, LF20-3, LF20-4, LF20-5) was 0.5–2 cm, with trending towards NE, and showed no obvious changes subsequently. In March 2015, a bulge emerged next to the reservoir bank.

In order to provide early-warning, measuring points and inclinometers were applied to the landslide for long-time professional monitoring. Fig. 2 shows part of measuring points displacement vectors and inclinometers. Table 1 shows the measuring points with the largest accumulated horizontal displacement in the active areas as of December 2015. Figs. 6–8, respectively, demonstrate the horizontal displacement and part of displacement rate of the Area LMG, Area CP1, and Area GBP1.

Subsequently, 12 measuring points and 12 inclinometers were established in Area LMG. Survey of boreholes reveal a wide distribution of colluvium, which can be divided into two sub-layers: (1) silt with gravel layer, with low bearing capacity, high clay content, and poor water permeability; (2) a high content of broken stone, with high porous, well water permeability and high bearing capacity. Fig. 6 shows the horizontal displacement and displacement rate (part of points) of measuring points in Area LMG. It can be seen from the figure that in 2013, the deformation of Area LMG was slow and steady, and then gradually decreased after its displacement rate peak in July 2014. In July 2015, the displacement
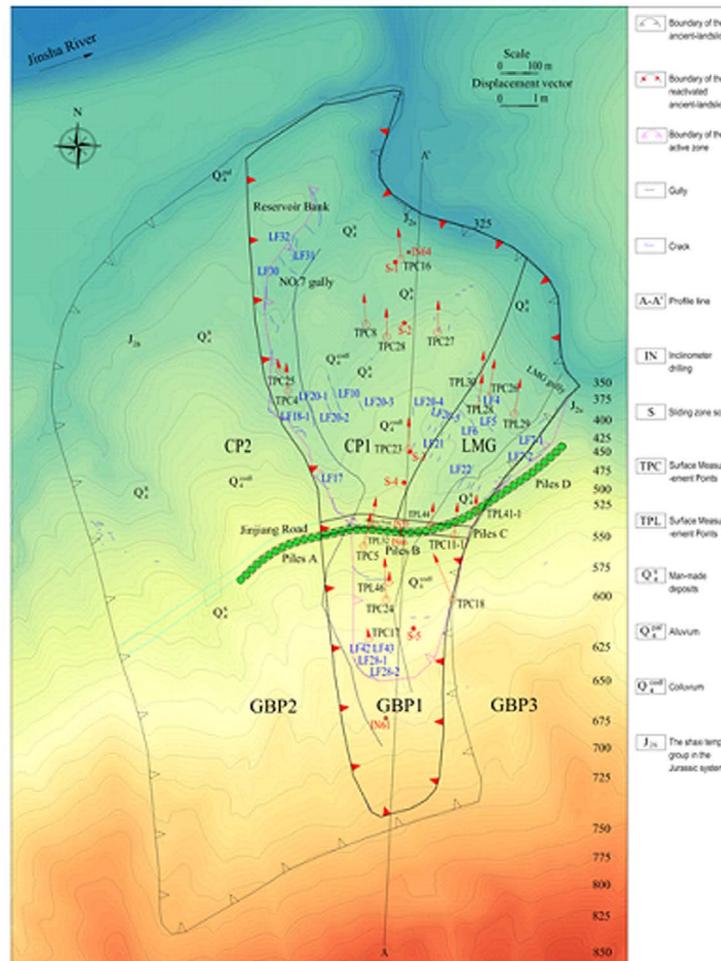
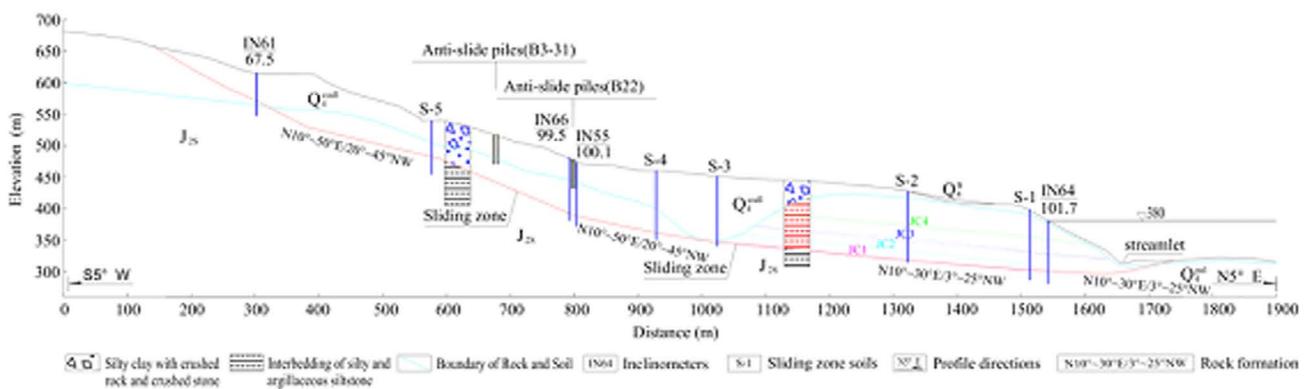Fig. 2. Geomorphological map of the research site, showing the monitoring network.

Fig. 3. Schematic geological cross-section (A-A') of the landslide.

rate increased once again, but did not exceed the peak value of 2014. The displacement rate of Area LMG fluctuated with time, but the overall trend corresponded to the horizontal displacement. The highest horizontal displacement monitoring point, TPL29, as of December 2015, with a horizontal displacement of 948 mm, a vertical displacement of 155 mm, and a maximum displacement rate of 4.13 mm d^{-1}.

Thereafter, 7 monitoring points and 12 inclinometers were established in Area CP1. Survey of boreholes reveals that the upper part is composed of the Q_4^{codl}, with a thickness of 1–100 m. The lower part is muddy intercalations and broken mud belts, with a maximum depth of over 100 m. Fig. 7 shows the horizontal displacement and displacement rate (part of points) of measuring points in Area CP1. In 2013,

Table 2
Configuration of selected inclinometer

Inclinometer No.	Depth of inclinometer (m)	Mouth elevation of inclinometer (m)	Elevation of sliding plane (m)	Sliding plane displacement (mm)	Ground water level (m)
IN61	67.5	614.86	567.86	11	604.46
IN66	99.5	480.7	390.2	5	476
IN55	100.1	471.9	387.82	10	472
IN64	101.7	380.7	300	16	380
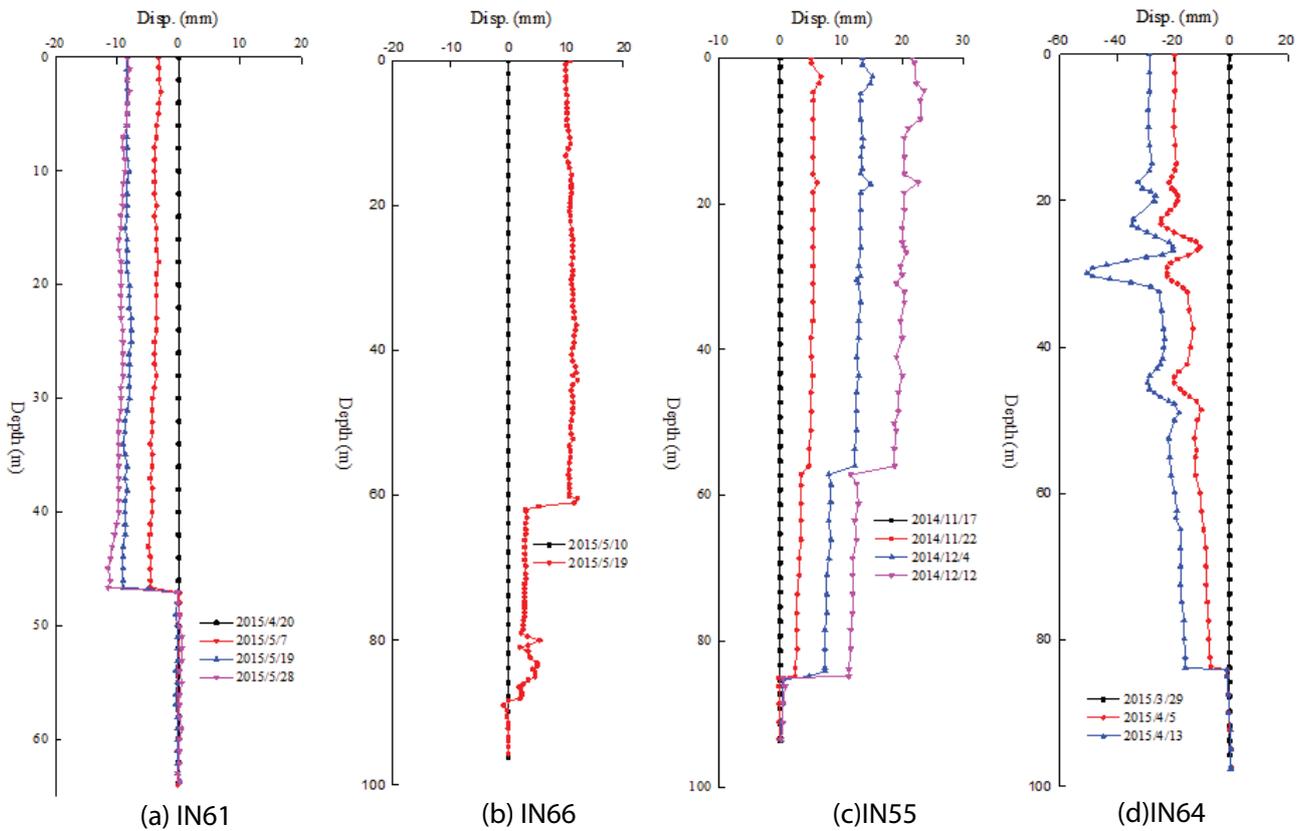
Fig. 4. Curves of displacement vs. depth indicated by inclinometer.

the deformation was small and the rate was stable. In May 2014, the deformation of each point increased sharply to a peak value. In 2015, the rate soared again, but did not exceed the maximum rate of 2014. Therefore, we may conclude that the overall displacement rate of Area CP1 was significantly volatile. The monitoring point, TPC23, with the highest horizontal displacement 848 mm as of December 2015, with a vertical displacement of 218 mm, and a maximum displacement rate of 2.14 mm d⁻¹.

In Area GBP1, 9 measuring points and 20 inclinometers were established. Survey of boreholes reveal a wide distribution of colluvium, which can be divided into two sub-layers: (1) silt with gravel layer, with low bearing capacity, high clay content and poor water permeability; (2) a high content of broken stone, with high porous and well water

permeability, the underlying rock mass is J_{2s} mudstone, which is relatively broken, with a high content of siltized intercalation, a rock inclination of 20°–45° which is moderate to strong weathering. Fig. 8 illustrates the horizontal displacement and displacement rate (part of points) of measuring points in Area GBP1. The deformation is relatively stable in 2013, and the trend in 2014 and 2015 is similar to that of Area LMG. The maximum displacement rate in 2015 is less than the peak value in 2014. The monitoring point, TPC18, with the highest horizontal displacement 1,480 mm as of December 2015, with a vertical displacement of 545 mm, and a maximum displacement rate of 3.84 mm d⁻¹.

In 2013, the deformation of active areas increased slowly with a rather stable rate, and the displacement rate of the Area LMG, Area CP1, and Area GBP1 were 0.62, 0.44, and
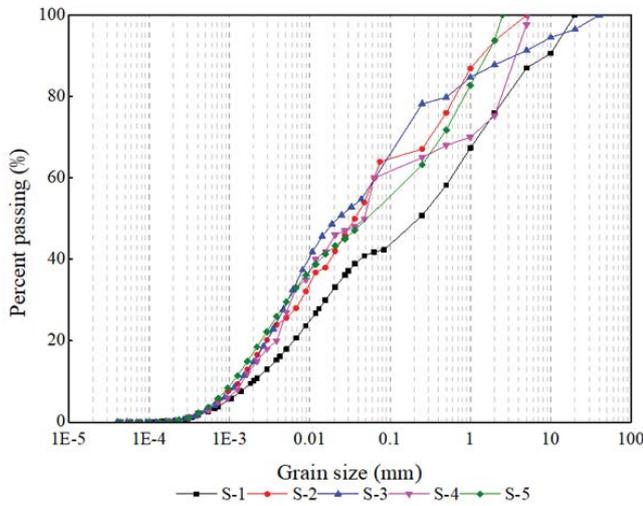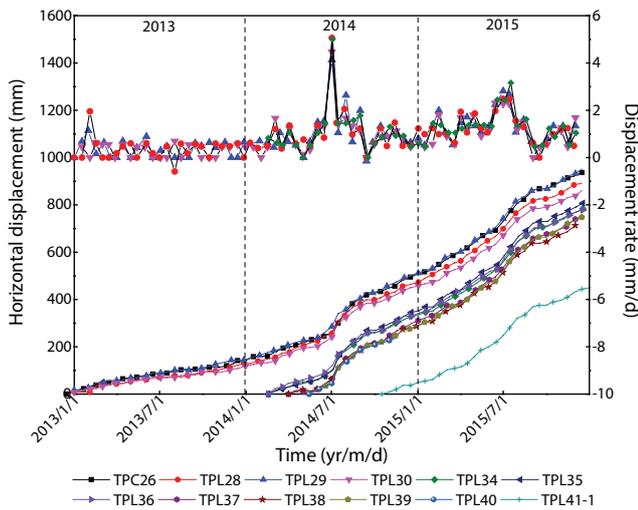
Fig. 5. Five grain size distribution curves.

Fig. 7. Horizontal displacement vs. time, displacement rate vs. time curves of CP1 during the monitoring.

Fig. 6. Horizontal displacement vs. time, displacement rate vs. time curves of LMG during the monitoring period.

Fig. 8. Horizontal displacement vs. time, displacement rate vs. time curves of GBP1 during the monitoring period.

0.63 mm d⁻¹, respectively. In 2014, the above three areas, respectively, had a highest displacement rate since 2013. The highest displacement rate is Area LMG (5.11 mm d⁻¹), followed by Area GBP1 (3.99 mm d⁻¹), and Area CP1 (3.15 mm d⁻¹). In 2015, the displacement rate in Area LMG was the highest (3.16 mm d⁻¹), followed by Area GBP1 (3.06 mm d⁻¹), and Area CP1 (2.85 mm d⁻¹). The deformation of Area GBP1 is greater than that of Area CP1 and the Area LMG. The horizontal displacement curves of measuring points in active areas reveal an evidently gradient shape whose height and grade increase with time. This phenomenon proves that the landslide deformation has been increasing on an annual basis.

This article defines the east as 0°, and takes the counterclockwise rotation as the deformation direction of measuring points. Some typical measuring points were selected to describe the relations between the deformed angle and
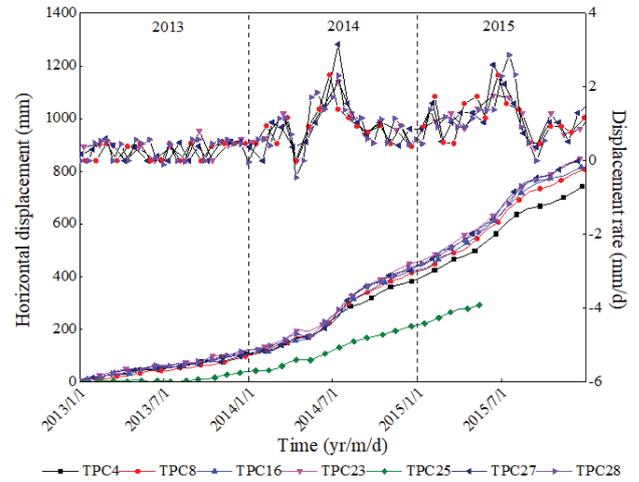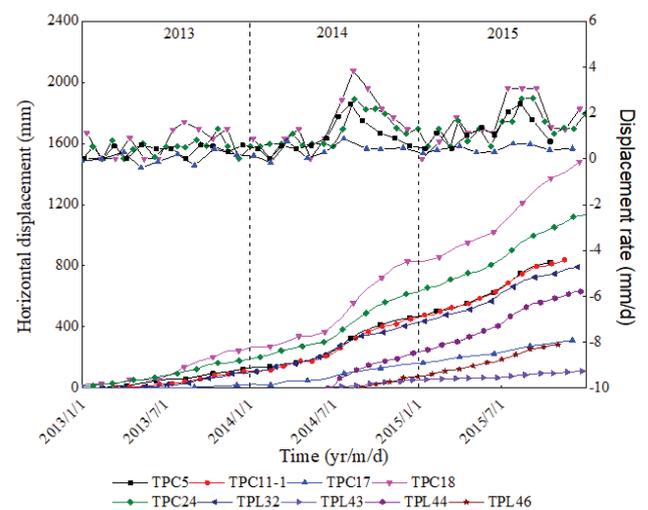
time (Fig. 9). Because of the ripping of landslide, TPC5 and TPC18 at the deformed boundary of Area GBP1 pointed towards the main slipping plane and have a trend of north. The TPC16, TPC23 and TPC26 began to move towards the north and had stabilized since September 2013. Judging from the curves, we can infer that the landslide underwent a dynamic process and then the slipping plane gradually cut through the whole landslide, finally towards the north (90°). Impacts of Area GBP1, the Area LMG and Area CP1 move towards the north. The horizontal displacement of Area LMG was greater than that of Area CP1, with a tendency of east, but the average direction was north. The deformation direction of Area CP1 is north, while the measuring points on the border are also close to the north.

The mouth cumulative displacement of inclinometers and horizontal displacement of measuring points during the same period are compared. The mouth displacement
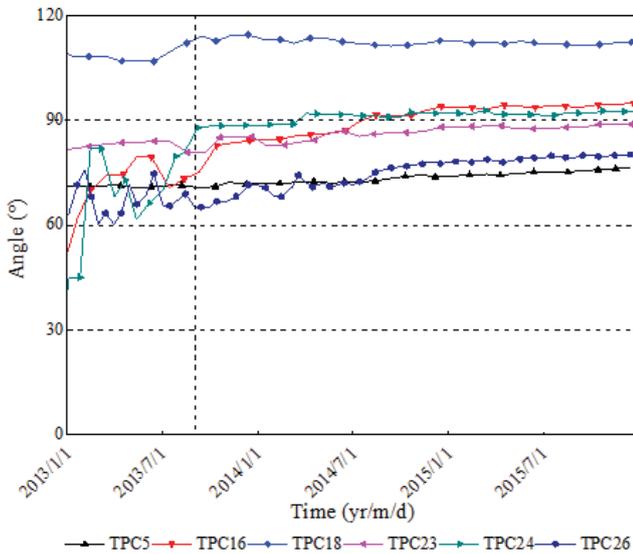
Fig. 9. Deformation angle vs. time curves of representative points during the monitoring period.

of IN61, IN66, IN55, and IN64 are coincident with that of measuring points displacement in general. That is to say, the displacement of ground and the in-depth displacement increase slowly and synchronously. It indicates that the ground deformation is caused by the in-depth deformation. The displacement of inclinometers dramatically change is the slipping plane. Impacts of Area GBP1, the Area CP1 and the Area LMG gradually deformed. The slipping plane passed through the JC1 muddy interlayer. The front of slope is empty, so the slipping plane reverse sheared out, resulting deformation and bulging in reservoir bank. There is a secondary shear in the slope, where stared from the IN66 to IN64. The slipping plane of Area GBP1's slope is 25°–30°, and the Area CP1's slope is 10°–15°.

Based on the results of horizontal displacement and the corresponding displacement rate, the main characteristics were observed as follows:

• The sliding directions of different areas were almost same. The displacement vectors of some measuring points are illustrated in Fig. 2. The deformation direction of Area GBP1 was right on the north (some points at the deformation boundary pointed towards the main slipping plane and converge to the north). The Area GBP1 pushed the Area CP1 and the Area LMG towards to north. There was a tendency to shift eastwards of Area LMG, but the average direction was right on the north.
• The deformation varied spatial. The vertical displacement and maximum displacement rate of the maximum horizontal displacement of monitoring pointed in different areas were shown in Table 1. The maximum displacement point's highest rate of Area LMG was 4.13 mm d^{-1}, and that of the Area CP1 was 2.14 mm d^{-1}, and the Area GBP1 was 3.84 mm d^{-1}. The eastern deformation of Area LMG was greater than those of western Area CP1. The deformation of Area GBP1 was greater than the Area CP1.

• The displacement rate fluctuated with time. In 2013, the displacement rate of Area LMG, CP1, and GBP1 was stable, with annual deformation values of 37.88–143.74, 38.11–108.76, and 20.33–243. 6 mm year^{-1}. In 2014, the annual deformation of the three areas grew rapidly to about 22.72–357.25, 172.73–339.18, and 53.69–584.03 mm year^{-1}. In 2015, annual deformation increased again in each area, which was about 75.76–462.06, 80.21–413.57, and 57.83–652.5 mm year^{-1}, respectively (Figs. 6–8). In 2014 and 2015, the displacement deformation curve showed a gradient shape, with a sharp increase in July, and the displacement rate reached its peak of each separate year. This phenomenon may be explained that the continuous creeping leads to excessive stress and strain energy, and they were released in 2014 and 2015 [26].
• Seasonal creep. The deformation was significant from June to September (rainy season) every year. The displacement rate was especially active in rainy season of 2014 and 2015. The maximum displacement rate in Area GBP1 was 3.99 mm d^{-1}, Area LMG was 5.11 mm d^{-1}, and Area CP1 was 3.16 mm d^{-1}. When winter approached, the displacement rate gradually decreased and tended to be stable (Figs. 6–8). The above phenomenon showed that rainfall was a crucial factor accelerating the deformation of landslide. Seasonal changes of landslide corresponded with the increase in recorded rainfall intensity. With the mounting rainfall, the displacement rate added up. The Area C was categorized as a seasonal creeping landslide [27].

4. Factors influencing the deformation of the landslide

The most essential reason why so many large-scale landslides developed in mainland China is the topography and landforms. While the strong earthquake, extreme climate, global climate change, and heavy rainfall trigger the occurrence of landslide [28,29]. A 3-year data show that rainfall intensity and reservoir water are the factors controlled the deformation of landslide.

4.1. Deformation is obviously affected by variation of the rainfall

Statistics related to the precipitation in active areas shows that the total annual rainfall in 2013, 2014, and 2015 amounted to 1,190. 4, 973.6, and 806.2 mm, respectively. The amount of rainy season accounted for 60%–75% of the annual precipitation. It was twice average monthly rainfall.

The displacement of measuring points from different active areas of the landslide has a good correlation with the variation of monthly rainfall (Fig. 10). The point where the displacement varies significantly corresponds to the point of rainfall intensity (July to September), which means, the displacement in response to the rainfall. For example, in October 2014, the widths of cracks LF7-1 and LF7-2 at the junction of Area LMG and Jinjiang Road opened from 5 to 50 cm after a rainfall intensity in 2015. In July 2014, the width of the cracks LF17 in Area CP1 opened from 5 to 15 cm after the rainy season in the same year. In July 2014, the width of cracks LF28-1 and LF28-2 in Area GBP1 opened from 3–5 cm to 25 cm after the rainy seasons of 2014 and 2015. Some of these expansive cracks occurred near the deformation boundary. After that the deformation progressed from local to global (Fig. 1).
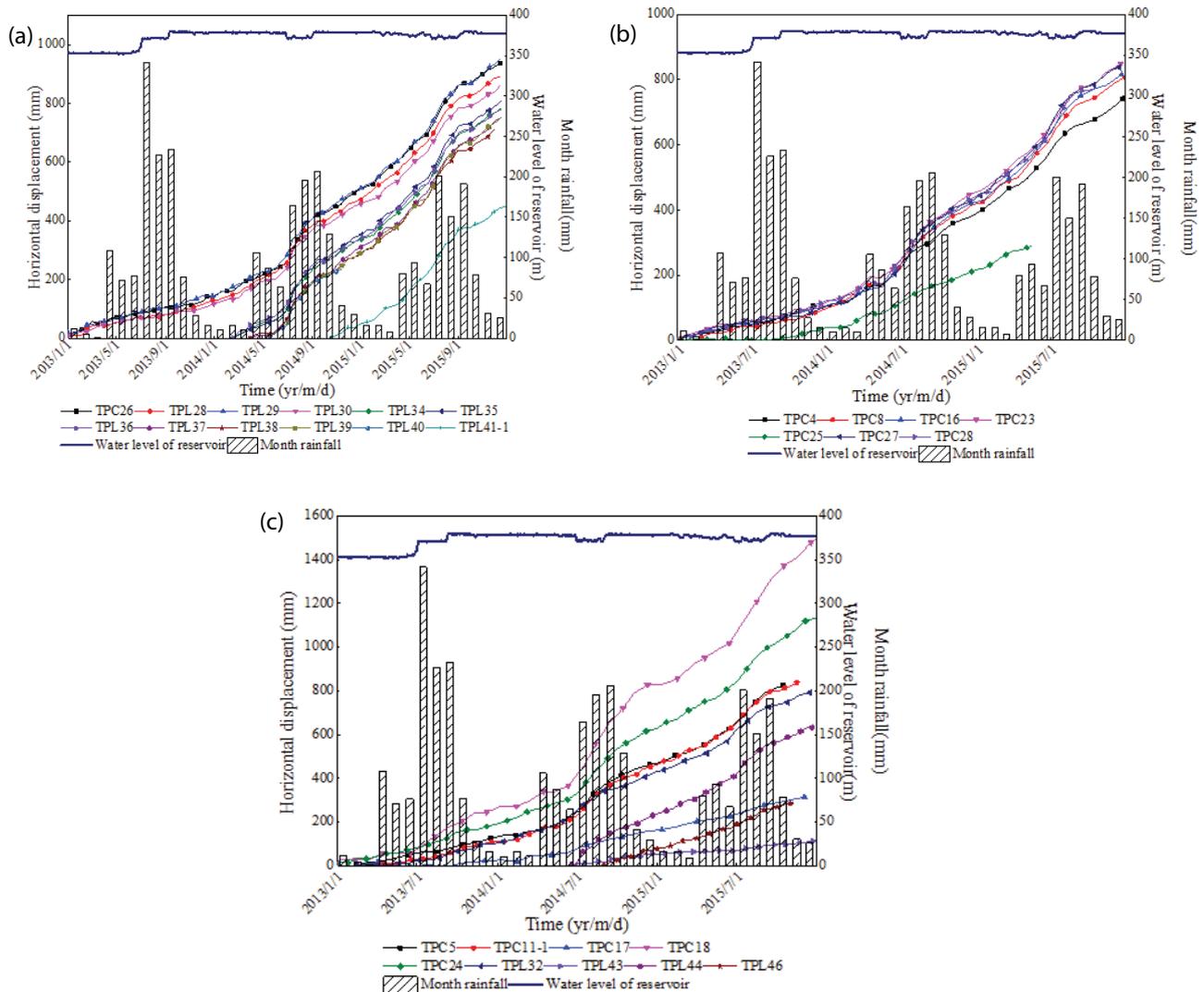
Fig. 10. Relationship between cumulative displacement, rainfall, and the reservoir water level (a) LMG, (b) CP1, and (c) GBP1.

4.2. Deformation is obviously affected by variation of the reservoir level

The water level of reservoir inundation phases I (October 2012), II (July 2013), and III (September 2013) were 354, 370, and 380 m, respectively. At the beginning of July every year, the water level of the reservoir fell to 370 m, and then resumed to 380 m in September every year.

According to the analysis of monitoring data, the deformation is affected by the fluctuation of reservoir water. The deformation is evidently affected by the drawdown of water level (Fig. 10). For instance, after rainy season in July 2013, the water level rose rapidly from 350 m in June to 380 m in September. The measuring points remained stable with no apparent acceleration. Because of the rising water level, the normal stress and pressure pused to landslide increased, prevented the deformation. At the beginning of July 2014, the water level fell from 380 to 370 m, while the deformation began in mid-June, which was prior to the falling of water reservoir. This phenomenon indicates that the impact

of reservoir water on deformation is small. Even under a amount of rainfall, the drawdown of reservoir water level is just an auxiliary factor. Therefore, we may infer that the deformation in 2013 was mainly caused by the rainfall, and the changes of reservoir water merely played a minor role. We may also conclude from Fig. 10 that the deformation of TPC16 at the front of landslide has a weakly correlation with the changes of water reservoir water level.

4.3. Combined effects of rainfall and water level

The rainfall and reservoir water are the two major factors that lead to the landslide deformation. It is evident that the deformation became more complex as a result of the coupling of rainfall and reservoir water. For example, from January to March in 2013, 2014, and 2015, the reservoir water levels were, respectively, 350, 380, and 380 m, and there was little precipitation. During these periods, deformation of landslide is rare. Thus, the influence of the reservoir water level on landslide deformation is rather weak. When the rainfalls

were strong, especially during the time when the reservoir water drawdown, the deformation of landslide was significantly evident. For example: the July to September in 2014 and 2015.

5. Mechanism of the deformation of the landslide

Based on the monitoring data and geographical researches of landslide, the mechanism deformation of Area *C* in Suijiang County could be analyzed as follows:

5.1. Rainfall is a major influence factor

Rainfall correlates with the horizontal displacement (deformation rate) significantly. To some extent, there is a positive correlation between rainfall and horizontal displacement (deformation rate), that is to say, the heavier rainfalls lead to the greater horizontal displacement (deformation rate).

The influences of rainfall that infiltrates into the interior of rock and soil are as follows: (1) the stress is uneven caused by mixed saturated and unsaturated soils. The soil with rich clay minerals are expansive due to increasing of water, and the mechanical parameters have changed with reduced shear strength; (2) the ground water level rises, altering the pore pressure; (3) the density of rock and soil increases, and the sliding force increases; (4) the rainfall infiltration is impeded by the impermeable interlayer, and rainwater flows along the surface of the interlayer, causing a greater crack.

5.2. Reservoir water is a minor factor

When the reservoir level changes, the rock and soil of landslide change between unsaturation with saturation, which cause reduction of cohesion and frictional angle. Lab experiment proves that when the material changes from the unsaturated state to saturated, the frictional angle is generally reduced by 10%–15%. And, the cohesion reduced too. The rock and soil in the front of landslide reach to saturation as the reservoir level rises, which cause reduced strength, plastic deformation, and low stability.

When reservoir water level is higher than groundwater level of slope, the reservoir water infiltrates into the slope, enhancing the landslide stability; when reservoir level drops, the underground water level of slope decreases with a lower speed, forming large hydraulic gradient oriented towards the outside of slope and increasing the sliding force, which decrease the stability.

5.3. Mechanism of deformation

The formation of Area C landslide is a complicated geographical and mechanical process. The B and C anti-slide pile plates suffer most of pressure transmitted from Area GBP1. The plates deform due to the excessive accumulation of stress and strain energy. Area GBP1 pushes Area LMG and Area CP1 deforms, especially the Area CP1 has a tendency to the sky.

The slope has gone through a cyclic process of "creep-accelerated deformation-stabilized deformation", which is shown as lapsing – cracking – shearing. During the rainfall intensity period in 2013, the Area GBP1 pushed the Area CP1

and Area LMG to deform. While the Area GBP1 was moving, the cracks and boundary sedimentation were rather obvious to identify. Subsequently, the slipping plane of Area GBP1 moved to north steadily [30,31]. After the rainfall intensity of 2014 and 2015, the Area GBP1 showed greater displacement than the Area CP1 and Area LMG, with an increasing deformation of crack and boundary sedimentation [32]. There are some feathered cracks on the boundary of Area LMG and Area CP1, the muddy intercalation which are affected by precipitation and reservoir water. The mechanical properties have been weakened. Slipping plane of Area CP1 formed and went through the most weakly muddy intercalation JC1. The whole slipping plane has formed by Area GBP1 and Area CP1. Then the landslide moved to north under the influence of rainfall and reservoir water. Terracette appeared at the rear of landslide [33–35]. The boundary of deformation had demonstrated more evidently at the rear of landslide. Radial cracks emerged at the front of landslide, and then sheared out of landslide after bending and bulging.

6. Conclusion

Based on the data of geological research of measuring points and inclinometers, the following conclusions are made:

- The terrain of south is higher than the north, suggesting a potential energy to support the deformation; the back rock is steeper than the front and the interbed of sand shale is soft-hard alternated, all these creating powerful qualifications for the forming of slipping plane; the cracks are well developed, providing a convenience to water penetration and transportation. The soil is rich in hydrophilic clay minerals with water-swelling, diminishing its mechanical properties and stability.
- The Area C is a reactivated ancient-landslide. The Area GBP1 and Area CP1 have formed a slipping plane and the slope continues to deform with time. The Area CP1 exists as a secondary slipping plane.
- The safety factor is 1.2 in natural condition, while the safety factor would drop to 0.99 in heavy rainfall and reservoir inundation.
- Influenced by the rainfall and reservoir water, the slope deformation is more evident, while the former one being the major influence factor. Impacted by the two cyclical factors, the mechanical properties and stability of landslide were diminished. During the rainy season, the deformation rate increases sharply, or the deformation rate will remain stable. The deformation is much more evidently affected by the drawdown of water level than the rising. When the rainfalls become more frequent, especially during the time when the reservoir water level drawdown, the deformation of landslide is significantly evident.
- The possibility of high-speed slip is very small. The Area C is categorized as a creeping landslide. The constant deformation will create a serious threat to the residents and the environment. Relevant measures should be taken to protect the safety of lives and properties in Area C. For example, we may eliminate or reduce the influence of water (rainfall and reservoir water), alter the geometry of rock and soil, and set up anti-slide tie.

Acknowledgement

References

[1] B. Voight, C. Faust, Frictional heat and strength loss in some rapid landslides: Error correction and affirmation of mechanism for the Vaiont landslide, Géotechnique, 42 (1992) 641–643.

[2] L. Muller, The Rock Slide in the Vajont Valley, J. Int. Soc. Rock Mech., 2 (1964) 148–212.

[3] H. Breth, The dynamics of a landslide produced by filling a reservoir, 9th International Congress on Large Dams, Istanbul, 1967, pp. 37–45.

[4] J. Corominas, J. Moya, Reconstructing recent landslide activity in relation to rainfall in the Llobregat River basin, Eastern Pyrenees, Spain, Geomorphology, 30 (1999) 79–93.

[5] F. Guzzetti, M. Cardinali, P. Reichenbach, Landslides triggered by the 23 November 2000 rainfall event in the Imperia Province, Western Liguria, Italy, Eng. Geol., 73 (2014) 229–245.

[6] T. Peng, G. Xu, D.Q. Xia, Trend of geological hazards and countermeasure of disaster reduction in the Three Gorges reservoir area, J. Mount. Sci., 22 (2014) 719–724.

[7] B.L. Huang, X.T. Chen, Deformation failure mechanism of Baijiabao layindslide in Xiangxi River Valley, Chin. J. Geotech. Eng., 29 (2007) 938–942.

[8] Q.L. Liao, X. Li, L. Souting Lee, Occurrence, geology and geomorphy characteristics and origin of Qianjiangping landslide in Three Gorges Reservoir area and study on ancient landslide criterion, Chin. J. Rock Mech. Eng., 24 (2005) 3146–3153.

[9] Y.P. Yin, X.M. Peng, Failure mechanism on Qianjiangping landslide in the Three Gorges Reservoir, Hydrogeol. Eng. Geol., 34 (2017) 51–54.

[10] D. Li, K. Yin, C. Leo, Analysis of Baishuihe landslide influenced by the effects of reservoir water and rainfall, Environ. Earth Sci., 60 (2010) 677–687.

[11] S.Q. Lu, Q.L. Yi, W. Yi, Study on dynamic deformation mechanism of landslide in drawdown of reservoir water level-take Baishuihe landslide in Three Gorges Reservoir area for example, J. Eng. Geol., 22 (2014b) 869–875.

[12] B.L. Huang, G.N. Liu, Y.P. Yin, Analysis of waves generated by Gongjiafang landslide in Wu Gorge, Three Gorges reservoir, on November 23, 2008, Landslides, 9 (2012) 395–405.

[13] L. Peng, R.Q. Niu, Analysis on deformation characteristics and influential factors of Baijiabao landslide in the Three Gorges Reservoir area, Chin. J. Geol. Hazard. Control, 22 (2011) 1–7.

[14] F. Wang, G. Wang, K. Sassa, Displacement Monitoring and Physical Exploration on the Shuping Landslide Reactivated by Impoundment of the Three Gorges Reservoir, China. Landslides: Risk Analysis and Sustainable Disaster Management, Proceedings of the First General Assembly of the International Consortium on Landslides, Springer, Berlin, 2005, pp. 313–319.

[15] F. Wang, Y.M. Zhang, Z. Huo, Movement of the Shuping landslide in the first four years after the initial impoundment of the Three Gorges Dam Reservoir, China, Landslides, 5 (2008) 321–329.

[16] S.Q. Lu, Q.L. Yi, W. Yi, Analysis of deformation and failure mechanism of Shuping landslide in Three Gorges reservoir area, Rock Soil Mech., 35 (2014) 1123–1130, 1202.

[17] S.Q. Lu, Q.L. Yi, W. Yi, Analysis on deformation and failure mechanism of Woshaxi landslide in the Three Gorges Reservoir Area, Adv. Mater. Res., 594–597 (2012) 498–501.

[18] J. Du, K.L. Yin, S. Lacasse, Displacement prediction in colluvial landslides, Three Gorges Reservoir, China Landslides, 10 (2013) 203–218.

[19] Z. Dai, Y. Yin, Y. Wei, Deformation an failure mechanism of Outang landslide in Three Gorges Reservoir area, J. Eng. Geol., 24 (2016) 44–55.

[20] A. Chybicki, Mapping south baltic near-shore bathymetry using sentinel-2 observations, Polish Marit. Res., 24 (2017) 15–25.

[21] M. Cruz Campas, A.G. Villalba Villalba, R. Ramirez Leal, Calidad Del Aire Respecto De Metales Relacion Con Salud Respiratoria: Caso Sonora, Mexico, Revista Int. Contaminacion Ambiental, 33 (2017) 23–34.

[22] D. Golui, S.P. Datta, S.C. Kaushik, Interferences of medium and matrix in determination of trace toxic elements using inductively coupled plasma mass spectrometry, J. Environ. Biol., 39 (2018) 103–108.

[23] D. Li, L. Wang, W. Peng, S. Ge, N. Li, Y. Furuta, Chemical structure of hemicellulosic polymers isolated from bamboo bio-composite during mold pressing, Polym. Compos., 38 (2017) 2009–2015.

[24] H.S. Lim, Open channel flow friction factor: logarithmic law, J. Coastal Res., 34 (2018) 229–237.

[25] A. Yang, Y. Han, S. Li, H. Xing, Y. Pan, W. Liu, Synthesis and comparison of photocatalytic properties for Bi_2WO_6 nanofibers and hierarchical microspheres, J. Alloys Compd., 695 (2017) 915–921.

[26] S. Qi, F. Yan, S. Wang, R. Xu, Characteristics, mechanism and development tendency of deformation of Maoping landslide after commission of Geheyan reservoir on the Qingjiang River, Hubei Province, China Eng. Geol., 86 (2006) 37–51.

[27] G.B. Crosta, F. Agliardi, Failure forecast for large rock slides by surface displacement measure, Can. Geotech. J., 40 (2003) 176–191.

[28] R.Q. Huang, Large-scale landslides and their sliding mechanisms in China since the 20th century, Chin. J. Rock Mech. Eng., 26 (2007) 433–454.

[29] Z.Q. Yin, Y.Q. Xu, W.J. Zhao, Sanxi village landslide in Dujiangyan, sichuan province on July 10, 2013, J. Eng. Geol., 22 (2014) 309–318.

[30] D. Sharma, K.D. Yadav, Application of rotary in-vessel composting and analytical hierarchy process for the selection of a suitable combination of flower waste, Geol. Ecol. Landscapes, 2 (2018) 137–147.

[31] W. Ennaji, A. Barakat, I. Karaoui, M.E. Baghdadi, A. Arioua, Remote sensing approach to assess salt-affected soils in the north-east part of Tadla plain, Morocco, Geol. Ecol. Landscapes, 2 (2018) 22–28.

[32] M. Foroozanfar, Environmental control in petroleum operations, J. CleanWAS, 1 (2017) 18–22.

[33] W.L. Wun, G.K. Chua, S.Y. Chin, Effect of Palm oil mill effluent (pome) treatment by activated sludge, J. CleanWAS, 1 (2017) 6–9.

[34] B. Andik, A. Sarang, Daylighting buried rivers and streams in Tehran, Water Conserv. Manage., 1 (2017) 1–4.

[35] H. Zarepourfard, A. Aryafar, H. Zia, The investigation of groundwater hydrochemistry of Khezri Plain, South Khorasan Province, Iran, Water Conserv. Manage., 1 (2017) 13–16.